C. T.-C. Nguyen, "Integrated micromechanical RF circuits for software-defined cognitive radio (invited plenary)," *Proceedings*, the 26th Symposium on Sensors, Micromachines & Applied Systems, Tokyo, Japan, Oct. 15-16, 2009, pp. 1-5.

Integrated Micromechanical RF Circuits for Software-Defined Cognitive Radio

Clark T.-C. Nguyen*

Abstract: An evaluation of the potential for MEMS technologies to realize the RF front-end frequency gating spectrum analyzer function needed by true software-defined cognitive radios is presented. Here, the relevant MEMS technologies include vibrating micromechanical resonators that exhibit record on-chip *Q*'s at GHz frequencies; medium-scale integrated micromechanical circuits that implement on/off switchable filter banks; and process technologies that integrate MEMS together with foundry CMOS transistors in a fully monolithic, low capacitance, single-chip process. Among the many issues that make realization of a frequency gating function a truly challenging proposition, e.g., resonator drift stability, mechanical circuit complexity, repeatability and fabrication tolerances, the need for resonators at GHz frequencies with simultaneous high *Q* (>30,000) and low impedance (e.g., 50Ω for conventional systems) is perhaps the most daunting. Some perspective on which resonator technologies, capacitive or piezoelectric, might best achieve these simultaneous attributes is also provided.

Keywords: micromechanical circuit, resonator, quality factor, wireless communications, filter, RF MEMS, motional resistance

1. Introduction

Recent advances in vibrating RF MEMS technology that yield on-chip resonators with *Q*'s over 10,000 at GHz frequencies [1][2] and excellent thermal [3] and aging stability [4], have now positioned vibrating micromechanical devices as strong candidates for inclusion into a number of future wireless communication sub-systems, from cellular handsets, to PDA's, to low-power networked sensors [5]. Indeed, early start-ups have already sprouted to take advantage of this technology for timekeeper applications, and the timing of this technology seems well placed for wireless markets, whose requirement for multi-mode reconfigurability fuels a need for on-chip high-*Q* resonators to prevent the cost of the front-end passives in a typical handset from obviating that of the integrated circuits (IC's) [5].

But the benefits of vibrating RF MEMS technology go far beyond mere component replacement. In fact, the extent of the performance and economic benefits afforded by vibrating RF MEMS devices grows exponentially as researchers and designers begin to perceive them more as building blocks than as standalone devices. In particular, when integrated into micromechanical circuits, in which vibrating mechanical links are connected into larger, more general networks, previously unachievable signal processing functions become possible, such as reconfigurable RF channel-selecting filter banks, ultra-stable reconfigurable oscillators, mechanical power converters, mechanical power amplifiers, frequency domain computers, and frequency translators. This paper focuses on the MEMS technologies most suitable to micromechanically realizing the frequency gating RF front-end needed by true software-defined cognitive radios.

2. Software-Defined Cognitive Radio

The increasing desire for reconfigurable radios capable of adapting to any communication standard at any location across the world has spurred great interest in the concept of a software defined radio (SDR) [6], in which the frequencies and modulation schemes of any existing communication standard can be produced in real-time by simply calling up an appropriate software sub-routine. Arguably, the ultimate rendition of such a radio would realize all radio functions, including the RF front-end, digitally, using a programmable microprocessor. To achieve this, the analog-to-digital converter (ADC) that normally resides near the baseband circuits of a conventional receiver would need be placed as close to the antenna as possible, so that as much signal processing as possible could be done digitally.

Ideally, the ADC would immediately follow the antenna and would have an input bandwidth covering the full spectrum of received signals, e.g., 3 GHz. Practically, however, a frequency gating function must precede the ADC to remove blockers (i.e., interferers) that can be many orders stronger than the desired signal at the receive antenna. Removing such blockers relaxes the ADC's dynamic range and power requirements, which otherwise would be too excessive for portable (and even stationary) applications. For reasonable power consumption, all interferers, even those close to the desired signal, must be removed.

To more concretely convey the importance of filtering out interferers before they reach the ADC input, Fig. 1 summarizes the dynamic range and consequential needed power consumption required by a state-of-the-art ADC used in an SDR under various bandwidths of filtering to remove interferers, and assuming a bit error rate of BER=10^{-6}. As shown, with no front-end filtering, the 0dBm blockers assumed in the GSM standard dictate an ADC dynamic range (DR) of 93dB. To attain this DR, the ADC would

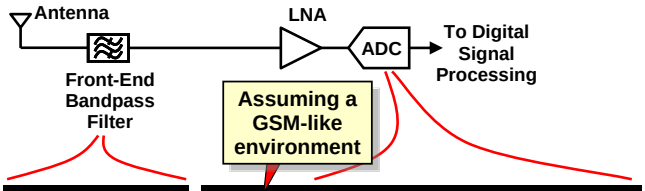

Filter Bandwidth	Largest Blocker	ADC DR Req'mt	# ADC Bits Req'd	Power Cons.
No Filter	0 dBm	93 dB	20	14.7 kW
35 MHz	-5 dBm	88 dB	18	3.68 kW
20 MHz	-23 dBm	70 dB	14	230W
6 MHz	-33 dBm	60 dB	11	28.8W
3.2 MHz	-43 dBm	50 dB	9	7.2W
Channel-Select	None	14.1 dB	3	~50 mW

Fig. 1: Dynamic range and consequent power consumption required by an ADC designed to accept a 3GHz-wide input RF spectrum for an SDR in a blocker environment identical to that assumed by the GSM standard.

* Dept. of EECS, University of California at Berkeley
Berkeley, California 94720, Email: ctnguyen@eecs.berkeley.edu

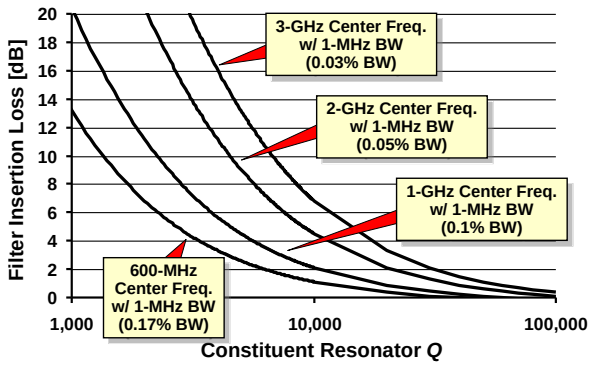

Fig. 2: Simulated plots of the insertion loss for 1-MHz bandwidth, 0.01dB ripple, 4-resonator Chebyshev filters at various frequencies versus the *Q*'s of their constituent resonators.

require 20 bits, which in recent transistor technology [7] would consume a whopping 14.7kW of power! Needless to say, without filtering, a wide-open ADC would be highly impractical.

As the bandwidth of filtering decreases, more interferers are suppressed, and the needed DR of the ADC relaxes. Note, however, from Fig. 1, that even the 35MHz bandwidth of a conventional pre-select filter (used in cell phones today) is still grossly insufficient for SDR, as the interferers that remain after its filtering still force the ADC to consume a still highly impractical 3.68kW. Indeed, as shown in Fig. 1, reasonable ADC power consumption on the order of 50mW is not achieved until the filter bandwidth corresponds to that needed to eliminate all interferers, i.e., to select the channel and only the channel. For GSM, where emissions are regulated so that each 200kHz channel is sandwiched by empty spectrum in any given cell, this would require a filter bandwidth of 600kHz, or a percent bandwidth on the order of 0.03%—two orders of magnitude smaller than the 3% of conventional pre-select filters!

It follows that to eliminate all interferers and pass only the desired signal, a programmable frequency gating device or circuit is needed that can pass and reject tiny (e.g., 0.03% bandwidth) RF frequency channels at will along the entire 3 GHz input frequency span. The need for such a small percent bandwidth makes this especially difficult, since the smaller the percent bandwidth, the higher the needed *Q*'s of the resonators comprising the filter to maintain reasonable insertion loss. Fig. 2 illustrates this point with plots of the insertion loss for 1-MHz bandwidth, 0.01dB ripple, 4-resonator Chebyshev filters at various frequencies versus the *Q*'s of their constituent resonators. As shown, the constituent resonators making up a 3-GHz, 0.03% bandwidth filter would require *Q*'s >30,000 just to maintain an insertion loss below 3dB. To further complicate things, it is often the case that the higher the *Q* of a resonator, the less tunable it is. In fact, at the time of this writing, there are no existing on-chip resonator technologies capable of achieving *Q*'s >30,000 while also being continuously tunable over a 3 GHz span.

Fortunately, MEMS technology offers an alternative method for achieving the desired programmable frequency gate that dispenses with the need to tune a given resonator's frequency over a wide range. In particular, being a wafer-level manufacturing technology similar to those used for integrated transistor circuits, MEMS encourages designers to use mechanical devices the same way transistors are used: in massive numbers. So instead of restricting the implementation of a programmable frequency gate to a single tunable filter, MEMS technology allows realization of

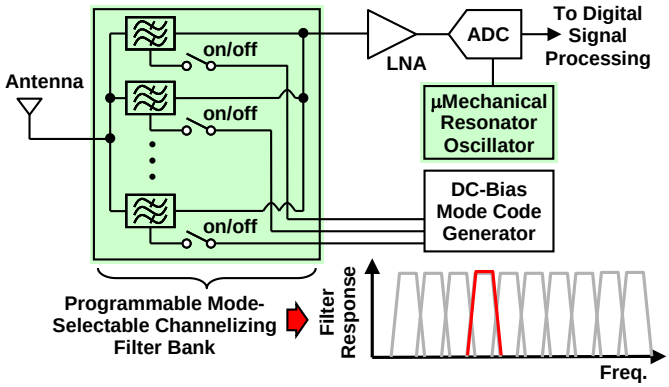

Fig. 3: System block diagram for a software defined radio front-end utilizing a micromechanical RF channel-select filter network to realize a frequency gating function. When one (or more) filters are turned "on", with all others "off", the filter bank realizes a frequency gate. When all filters are turned "on", the bank realizes a real-time spectrum analyzer that could be used to assess the entire received spectrum and determine what frequencies might be permissible to operate a cognitive radio.

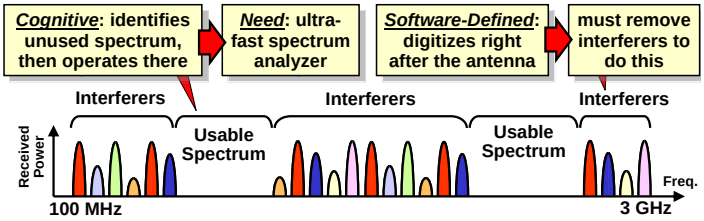

Fig. 4: Cartoon of the typical power spectrum that might be received by an antenna-terminated spectrum analyzer atop a tall building at a given moment in time.

the same programmable frequency gate via a bank of on/off switchable micromechanical filters, as depicted in Fig. 3, where each filter is realized using an interconnected network of micromechanical disk resonators.

2.1 Cognitive Radio

The programmable frequency gate of Fig. 3 is not only applicable to SDR, but also to cognitive radio. In particular, beyond SDR, many researchers are further exploring the possibility of a cognitive radio that is not restricted to operation only in a prescribed frequency band (which is the situation today), but that can seek out unused spectrum and operate there until a higher priority user shows up, in which case the radio must move to another unused frequency. Such a scheme recognizes that although the entirety of available spectrum has already been allocated to someone (or some purpose) by a regulating body, e.g., the Federal Communications Commission (FCC) in the U.S., the prescribed users do not always use their spectrum. In particular, the actual used spectrum at any given moment in time might look as shown in Fig. 4, which plots a cartoon of the typical power spectrum that might be received by an antenna-terminated spectrum analyzer atop a tall building at a given moment in time. As mentioned, a cognitive radio would seek to operate in any one of the empty bands, labeled "usable spectrum". However, in order to determine which bands are empty, such a radio would need to first be able to take a snapshot of the power spectrum. This would require a spectrum analyzer and a very fast one at that, since the cognitive radio would need to check spectrum usage every few milliseconds in order to know when to vacate a chan-

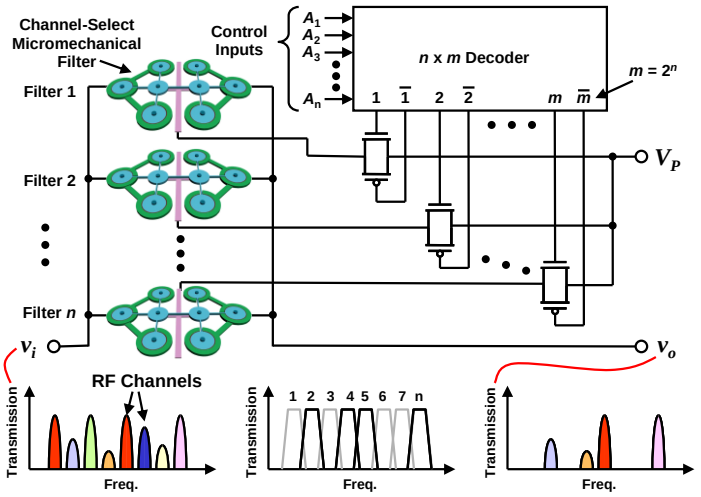

Fig. 5: Schematic of an RF channel-select micromechanical filter bank, with an example showing how various input frequencies can be simultaneously selected via mere application or removal of resonator dc-biases. In the bottom plots, filters 2, 4, 5, and *n* are on, while all others are off.

nel when a higher priority user begins to use it. Thus, the needed spectrum analyzer must both be extremely fast and consume very little power in portable handheld applications.

Unfortunately, presently available methods for spectrum analysis cannot achieve both speed and lower power simultaneously. In particular, fast spectrum analyzers based on FFT circuits would require excessive power to cover a 3GHz band; and lower power swept filter spectrum analyzers cannot sweep their filters faster than a time determined by the filter settling time, so are not fast enough. On the other hand, MEMS technology seems very well suited to this problem. In particular, the very mechanical circuit of Fig. 3 that implements a frequency gate also functions as a spectrum analyzer when all of its filters are turned on simultaneously. The resulting spectrum analyzer is both extremely fast, since little or no filter sweeping would be needed; plus very low in power consumption, since it is virtually all passive. As a result, the micromechanical circuit of Fig. 3 realizes both the frequency gating needed for SDR and the fast, low-power spectrum analyzer needed for cognitive radio, and hence, effectively realizes what might be called a frequency gating spectrum analyzer well tailored for software defined cognitive radio.

Of course, such a mechanical circuit is only useful if simultaneous high-*Q* and low impedance can be obtained; if switching of filters can be done quickly and without additional insertion loss; and if MEMS fabrication technology can support a VLSI mechanical circuit. Examples of MEMS technologies that might address these issues and make possible the described frequency gating spectrum analyzer are now presented.

3. Micromechanical Programmable Frequency Gating Spectrum Analyzer

Fig. 5 presents a more detailed schematic showing one approach to implementing the frequency gating spectrum analyzer of Fig. 3 using as building blocks capacitively transduced micromechanical disk resonators. Fig. 6 presents the SEM and measured frequency characteristic for one such resonator: a 1.51-GHz radial-contour mode disk resonator that achieves an impressive on-chip room temperature *Q* of 11,555 in vacuum, and 10,100 in air [2]. This device consists of a 20μm-diameter, 3μm-thick polydiamond disk suspended by a polysilicon stem self-

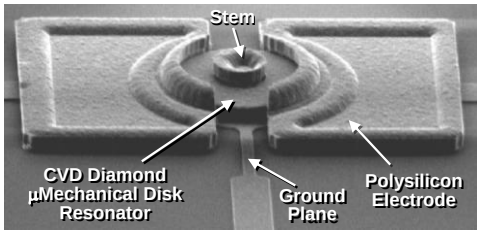

Fig. 6: SEM of a 1.51-GHz μmechanical radial mode disk resonator.

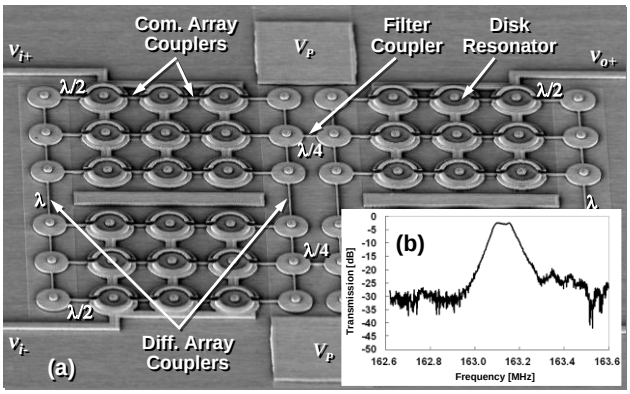

Fig. 7: (a) Mechanical circuit realizing a mode-switchable filter bank that performs the frequency gating function of Fig. 3. (b) Measured passband frequency characteristic for the lowest frequency mode.

aligned to be exactly at its center, all enclosed by doped polysilicon electrodes spaced less than 80 nm from the disk perimeter. It can be excited into resonance via a combination of dc and ac voltages that can be chosen to turn the device "on" or "off" [1][8], very conveniently realizing the switchability required by the circuits of Fig. 3 and Fig. 5. When vibrating in its radial contour mode, the disk expands and contracts around its perimeter, in a motion reminiscent of breathing, and in what effectively amounts to a high stiffness, high energy, extensional mode. Since the center of the disk corresponds to a node location for the radial contour vibration mode shape, anchor losses through the supporting stem are greatly suppressed, allowing this design to retain a very high *Q* even at this UHF frequency. A version of this device at 498 MHz achieves a *Q* of 55,300 in vacuum [2], which is more than enough to implement the needed tiny percent bandwidth filters for the described RF frequency gating spectrum analyzer.

Recognizing this, Fig. 7(a) presents a mechanical circuit fabricated via the process of [9] that realizes a switchable bank of side-by-side mechanical filter passbands, each selectable by dc-bias voltages applied to the resonators that form them. As shown, this mechanical circuit is comprised of several identical resonator elements coupled by mechanical links of various designed lengths attached at very specific locations on the resonators. Briefly, the center frequency of each switchable passband is determined primarily by the (identical) frequencies of the constituent resonators vibrating in the mode corresponding to the selected passband; while the bandwidths of the passbands and the spacings between them are determined largely by ratios of the stiffnesses of the various coupling beams to those of the resonators they couple at the attachment locations. Fig. 7(b) presents a measurement of the lowest frequency switched-mode passband, which has a 0.06% bandwidth with a 2.43dB insertion loss.

The complete structure of Fig. 7(a) comprises a medium-scale integrated (MSI) mechanical circuit that can be equated to an equivalent electrical circuit [9], with a one-to-one correspon-

dence between mechanical and electrical elements. The values of the circuit elements are specified by the lateral dimensions of the associated mechanical elements, so the whole structure is amenable to automatic generation by a computer-aided design (CAD) program. Such a program could also automatically generate the layout required to achieve a specific filter specification, making the realization of a VLSI circuit of such filters as convenient as for VLSI transistor IC's.

4. Impedance Matching

Unfortunately, although the *Q*'s of these resonators are exceptional, they are not easy to access, because the impedances they present are often much larger than that of the system that uses them. For example, many of today's board-level systems are designed around 50Ω impedance, which is much smaller than the 2.8kΩ termination resistors required by the 163-MHz differential disk array filter of [9]. Thus, even though the filter of [9] attains an impressively low insertion loss for a 0.06% bandwidth, it requires an *L*-network to match to 50Ω.

One possible solution to this impedance problem is to use piezoelectric micromechanical resonators, such as the AlN one of [10], which achieves a single resonator impedance of 80Ω. However, it posts a *Q* of only 2,900. Wafer-bonded thin quartz resonators have achieved *Q*'s of 14,756 at 545MHz, and 7,544 at 2.72GHz [11], but these are still far short of the 30,000 needed for channel-selection at RF. With further research, it is not unreasonable to expect that the *Q*'s of thin-film piezoelectric resonators should eventually increase. Still, capacitive resonator *Q*'s are already sufficient for RF channel-selection. So the question is: Which is easiest to do: Raise the *Q* of piezoelectric resonators; or reduce the impedance of capacitive resonators?

Recently published work asserts that the latter seems easier and is in fact happening quite rapidly. Indeed, several approaches are available that lower the motional resistance R_x of a capacitive resonator, all identifiable by simply studying its approximate expression:

$$R_x = \frac{\omega_o m_r}{Q} \cdot \frac{1}{V_P^2} \cdot \frac{d_o^4}{(\varepsilon A_o)^2} \qquad (1)$$

where ω_o and m_r are the radian resonance frequency and equivalent mass, respectively, of the resonator; A_o and d_o are the electrode-to-resonator overlap area and gap spacing, respectively; V_P is the dc-bias applied to the resonator's conductive structure; and ε is the permittivity in the electrode-to-resonator gap. From (1), the value of R_x can be lowered by raising the dc-bias voltage V_P; increasing the electrode-to-resonator overlap area A_o [12]; increasing the electrode-to-resonator gap dielectric constant ε [13][14]; and reducing the electrode-to-resonator gap d_o [15]. Clearly, by virtue of its fourth power dependence, the last of these is most effective. This is true not just for reducing motional resistance, but also more importantly, for maximizing the mechanical filter figure of merit *FOM*, given by

$$FOM = \frac{1}{R_Q C_o} = \frac{q}{m_r B} \cdot \frac{\varepsilon A_o}{d_o^3} \qquad (2)$$

Where R_Q is the needed filter termination resistance, C_o is the input overlap and shunt capacitance, q is a constant specific to the filter design, e.g., Chebyshev, Butterworth, 4–resonator, etc., obtainable from a filter cookbook; and B is the filter bandwidth. The *FOM* is more useful than R_x for gauging efficacy in an actual RF filter, since it accounts for the interaction between motional resistance and input shunt capacitance C_o. From (2), decreasing gap spacing increases the *FOM* much faster than other impedance-reducing approaches.

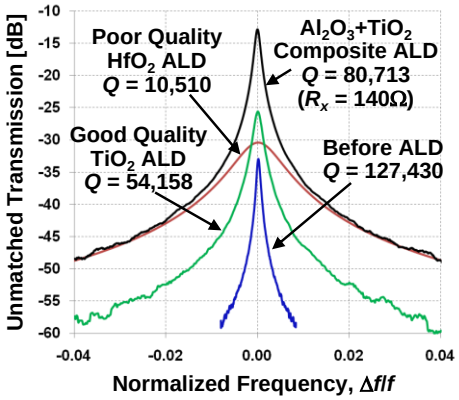

Fig. 8: Measured frequency spectra for 61-MHz wine-glass disk resonators with partial-filled gaps attained via various ALD recipes. The most recent recipe combines Al_2O_3 and TiO_2 ALD to achieve the smallest surface loss condition, allowing the resonator to achieve Q >80,000 while simultaneously posting R_x <200Ω—the first of its kind.

And contrary to popular belief, reducing gap spacing does not impact linearity as adversely as some may think. This can easily be seen from the experimentally verified expression for the third-order intermodulation input intercept point IIP_3 from [16]. For a 3μm-thick 1-GHz radial-contour mode polysilicon disk resonator with a radius of 2.64μm, dc-bias V_P of 10V, and Q = 50,000, the IIP_3 expression from [16] predicts that simply changing gap spacing from 80nm to 30nm actually increases, not decreases, the IIP_3, from 25.1dBm to 28.0dBm, respectively! The reason for this is that although a reduction in gap spacing does indeed reduce the permissible amplitude of vibration, it also substantially reduces the R_x, so the amplitude of vibration needed to support a given power level is also much smaller.

Among methods for reducing gap spacing, the partial ALD gap-filling approach of [15] is very attractive, since it not only reduces the effective gap spacing but also introduces a dielectric into the gap that prevents shorting of the resonator to its electrode. The work of [15], however, was plagued by additional energy dissipation from the ALD film that substantially lowered the *Q* of a 61-MHz wine-glass disk resonator, from its uncoated 150,527 to only 10,510 after ALD coating and sintering. Recent advances, however, in the ALD gap-filling technology have yielded much higher *Q*'s, as shown in Fig. 8, producing for the first time single resonators with simultaneous *Q*'s >80,000 and motional resistance <200Ω. With simple arraying, such as demonstrated in [12], the motional resistance can be reduced several fold, to 20Ω or lower.

At GHz frequencies, however, merely reducing the gap spacing is generally not sufficient if 50Ω is desired. Indeed, (1) shows that R_x increases linearly with frequency. To circumvent this, one need only use a mechanical circuit, such as an array. Indeed, at 1 GHz, 50Ω can be achieved using a mechanically coupled array 24 of 3μm-thick, 2.64μm-radius, 50,000-*Q* polysilicon disks, each with V_P = 10V and 30nm electrode-to-resonator gap spacings, all occupying a total die area of only 45×29μm^2 and possessing a substantially better IIP_3 than that of a single disk.

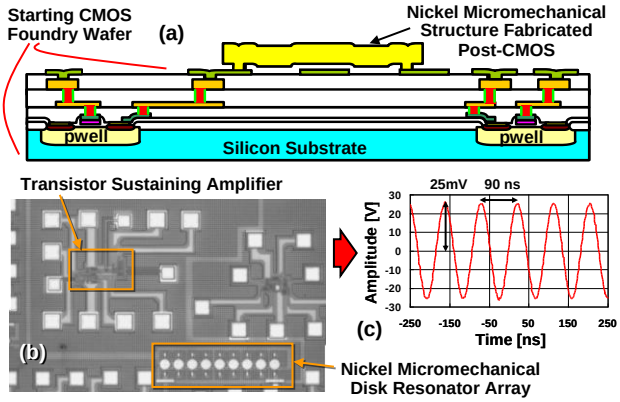

Fig. 9: (a) Cross-section of the nickel MEMS-transistor integration process of [18]. (b) Die photo of a fully monolithic micromechanical resonator oscillator using this process. (c) Oscilloscope waveform.

5. MEMS-Transistor Integration

Although Fig. 8 speaks well to the potential for capacitive resonators to achieve 50Ω with simultaneous *Q*'s >30,000, such a low impedance likely will not be needed in the future. In particular, although 50Ω is required by off-chip board-level implementations, it is not necessary for fully integrated single-chip solutions. Indeed, once micromechanical filters are integrated together with transistors on single silicon-chips, impedance requirements will very likely grow to the kΩ range for best performance [5]. And integration is likely a must for the circuit of Fig. 3, which does not explicitly show the transistor circuits needed to route the bias voltages that select (i.e., turn "on") the desired passbands. Given the complexity and density of the MEMS-to-transistor interconnections needed, it would be best if the MEMS and transistors were integrated together onto a single chip. Among approaches to doing this, MEMS-last ones are perhaps the most attractive, since they allow the use of virtually any foundry for transistor circuits.

To date, however, MEMS-last integration approaches have had little traction in consumer markets, partly because they require that processing temperatures for the MEMS stay below a ceiling that insures minimal degradation in transistor performance. Very few of the popular high-*Q* materials used for MEMS resonators, including the polydiamond and polysilicon materials of Fig. 6 and Fig. 7, are doable at temperatures under the needed ceiling, which may soon be around 300°C to accommodate the advanced low-k interconnect dielectrics targeted for future CMOS generations [17]. Recent work, however, has shown (to the surprise of many) that metal materials can achieve high *Q* at high frequencies as long as the right resonator designs (e.g., disk geometries) are utilized [18]. Specifically, wine-glass disk resonators with *Q*'s >50,000 have now been demonstrated in nickel material electroplated at only 50°C. Capitalizing on this discovery, Fig. 9 presents the cross-section, die photo, and oscilloscope output waveform for a fully monolithic single-chip micromechanical resonator oscillator that combines nickel MEMS over foundry CMOS, recently demonstrated with reasonable high-*Q* oscillator performance [18]. With this, it may not be too long before top-level CMOS metals are used to implement micromechanical circuits, such as that of Fig. 7, allowing the whole system of Fig. 3 to reside on a single tiny silicon-chip.

6. Conclusions

The recent demonstration of micromechanical resonators capable of posting simultaneous high *Q* >30,000 and low impedance <200Ω now encourages the use of MEMS technology to address the needs of future software-defined cognitive radios. Much work still remains to control of drift, manage complexity and repeatability for VLSI mechanical circuits, and lower the cost of MEMS-transistor integration, but vibrant research efforts are already underway to address these issues.

Acknowledgement: Much of the work summarized was supported by funding from DARPA.

References.

[1] S.-S. Li, *et. al.*, "Micromechanical hollow-disk ring resonators," *Proceedings*, 17th IEEE Int. MEMS Conf., Maastricht, The Netherlands, Jan. 25-29, 2004, pp. 821-824.

[2] J. Wang, *et al.*, "1.51-GHz polydiamond micromechanical disk …," *Proceedings*, 17th IEEE Int. MEMS Conf., Maastricht, The Netherlands, Jan. 25-29, 2004, pp. 641-644.

[3] W. -T. Hsu and C. T. -C. Nguyen, "Stiffness-compensated temperature-insensitive micromechanical resonators," *Tech. Digest*, IEEE Int. MEMS Conf., Las Vegas, NV, Jan. 20-24, 2002, pp. 731-734.

[4] B. Kim, *et. al.*, "Frequency stability of wafer-scale encapsulated MEMS resonators," *Digest of Technical Papers*, Transducers'05, Seoul, Korea, June 2005, pp. 1965-1968.

[5] C. T.-C. Nguyen, "MEMS technology for …," *IEEE Trans. Ultrason., Ferroelect., Freq. Contr.*, vol. 54, no. 2, pp. 251-270, Feb. 2007.

[6] M. Dillinger, *et al., Software Defined Radio: Architectures, Systems, and Functions*. New York, NY: Wiley, 2003.

[7] National Semiconductor ADC083000 Data Sheet.

[8] S.-S. Li, *et. al.*, "Self-switching vibrating micromechanical filter bank," *Proceedings*, Joint IEEE Int. Frequency Control/PTTI Symposium, Vancouver, Canada, Aug. 29-31, 2005, pp. 135-141.

[9] S.-S. Li, *et al.*, "An MSI micromechanical … filter," *Dig. of Tech. Papers*, Transducers'07, June 11-14, 2007, pp. 307-311.

[10] G. Piazza, *et. al.*, "Low motional resistance ring-shaped contour-mode aluminum nitride piezoelectric micromechanical resonators for UHF applications," *Tech. Dig.*, 18th IEEE Int. Conf. on MEMS, Miami Beach, Florida, Jan. 30-Feb. 3, 2005, pp.20-23.

[11] F. P. Stratton, *et. al.*, "A MEMS-based quartz resonator technology for GHz applications," *Proceedings*, IEEE Int. Ultrasonics, Ferroelectrics, and Frequency Control 50th Anniv. Joint Conf., Montreal, Canada, Aug. 24-27, 2004, pp. 27-34.

[12] M. Demirci and C. T.-C. Nguyen, "Mechanically corner-coupled square microresonator array for reduced … resistance," *IEEE/ASME J. Microelectromech. Syst.*, vol. 15, no. 6, pp. 1419-1436, Dec. 2006.

[13] Y.-W. Lin, *et. al.*, "Vibrating … resonators with solid dielectric capacitive-transducer 'gaps'," *Proceedings*, Joint IEEE Int. Freq. Control/PTTI Symp., Vancouver, Canada, Aug. 29-31,2005, pp. 128-134.

[14] D. Weinstein, *et. al.*, "Dielectrically transduced single-ended to differential MEMS filter," *Tech. Digest*, 2006 IEEE Int. Solid-State Circuits Conf., San Francisco, CA, February 5-9, 2006, pp. 318-319.

[15] L.-W. Hung, *et. al.*, "Capacitive transducer … via ALD-enabled partial-gap filling," *Tech. Digest*, 2008 Solid-State Sensor, Actuator, and Microsystems Wkshp, Hilton Head, SC, June 1-5, pp. 208-211.

[16] Y.-W. Lin, S.-S. Li, Z. Ren, and C. T.-C. Nguyen, "Third-order intermodulation distortion in … resonators," *Proceedings*, IEEE Int. Ultrasonics Symposium, Sept. 18-21, 2005, pp. 1592-1595.

[17] G. Maier, "The search for … ultra-low-k dielectrics: …," *IEEE Electrical Insulation Magazine*, vol. 20, no. 2, pp. 6-17, Dec. 2004.

[18] W.-L. Huang, *et al.*, " Fully monolithic CMOS nickel μmechanical …, " *Tech. Digest*, IEEE MEMS Conf., Jan. 13-17, 2008, pp. 10-13.